

Estimation of Parameters for an Archetypal Model of Cardiomyocyte Membrane Potentials

Muhamad H.N. Aziz¹, Radostin D. Simitev^{2*}

¹*Institute of Mathematical Sciences
University of Malaya
50603 K. Lumpur
Malaysia
E-mail: hifz_din@um.edu.my*

²*School of Mathematics and Statistics
University of Glasgow
Glasgow G12 8QQ
United Kingdom
E-mail: Radostin.Simitev@glasgow.ac.uk
orcid.org/0000-0002-2207-5789*

* *Corresponding author*

Received: filled by editor

Accepted: filled by editor

Published: filled by editor

Abstract: *Contemporary realistic mathematical models of single-cell cardiac electrical excitation are immensely detailed. Model complexity leads to parameter uncertainty, high computational cost and barriers to mechanistic understanding. There is a need for reduced models that are conceptually and mathematically simple but physiologically accurate. To this end, we consider an archetypal model of single-cell cardiac excitation that replicates the phase-space geometry of detailed cardiac models, but at the same time has a simple piecewise-linear form and a relatively low-dimensional configuration space. In order to make this archetypal model practically applicable, we develop and report a robust method for estimation of its parameter values from the morphology of single-stimulus action potentials derived from detailed ionic current models and from experimental myocyte measurements. The procedure is applied to five significant test cases and an excellent agreement with target biomarkers is achieved. Action potential duration restitution curves are also computed and compared to those of the target test models and data, demonstrating conservation of dynamical pacing behaviour by the fine-tuned archetypal model. An archetypal model that accurately reproduces a variety of wet-lab and synthetic electrophysiology data offers a number of specific advantages such as computational efficiency, as also demonstrated in the study. Open-source numerical code of the models and methods used is provided.*

Keywords: *Mathematical models, Cardiac action potential, Electrophysiology, Parameter estimation.*

Introduction

Models of the action potential of cardiac cells are routinely used to interpret and integrate experimental findings, extrapolate animal data to human system context, and test novel hypotheses [21, 51]. It is frequently proposed that these models will soon make it possible to devise patient-specific precision therapies, and accelerate cardiac drug discovery and development [3, 16, 50]. Since the pioneering work of Noble [37], over 150 models have been published with the aim to capture in detail the electrophysiology of a wide variety of cardiac cell types under a broad range of experimental, physiological and pathological conditions [19]. Contemporary detailed models largely follow the Hodgkin-Huxley paradigm but have grown to a staggering complexity [44]. For example, a recent model of the human ventricular action potential [39] consists of 49 ordinary differential equations and includes 206 model parameters. Because models are typically developed by extending and re-using components from previous models, as advocated by large international initiatives like the Physiome Project [6] and the CellML Project [30],

many of these parameters and equations are poorly constrained and in many cases redundant. For instance, the meta-analysis of [36] demonstrates that the modern human ventricular models [48, 22] include parameters that have been inherited from studies in at least 9 different species over a range of 6 different temperatures; in other words, it is questionable whether they represent any human ventricular myocyte. While intense research effort is expended to estimate parameter uncertainty [12], calibrate models to identifiable and reliable experimental protocols [55, 13], increase reproducibility [14] and build trustworthy models [23], detailed cardiac cell models remain difficult to benchmark and to adapt to situations to which they have not been fitted [56] and are computationally expensive especially in tissue-scale simulations [11]. Most importantly, detailed cardiac models are becoming increasingly difficult for causal inference [9].

Thus, there is a certain need for simplified mathematical models that are accurate and flexible enough, computationally affordable, amenable to mathematical analysis and to mechanistic understanding. Starting with the early work of van der Pol [53] a number of conceptual models have been proposed to address this need, e.g. [20, 34, 2, 18, 31], and most of them have become popular and frequently used in the place of detailed ones. However, these conceptual models rely mostly on ad hoc assumptions and generally have a FitzHugh-Nagumo structure that leads to certain shortcomings [9]. In contrast, in [10, 9] we developed an asymptotic method that allows for a systematic and controlled reduction of arbitrary detailed cardiac ion current models. The method preserves the phase-space geometry of detailed models, different from the FitzHugh-Nagumo one, and reveals qualitatively new features of topological nature [45]. Following this approach in [9] we reduced Noble's model of purkinje fibre electrophysiology [37]. We obtained a mathematically simple conceptual model that consists of three piece-wise linear differential equations and contains only 13 intrinsic model parameters and so it is rather inexpensive to integrate numerically. Further, the model admits closed-form analytic solutions when spatially-clamped [9], and closed-form travelling wave solutions when spatially-extended [45]. These exact solutions aid mechanistic understanding, extensive exploration of parameter space as well as benchmarking of numerical codes. More importantly the model is archetypal in the sense that it has the generic asymptotic structure of modern detailed cardiac ionic models and it is thus capable of reproducing slow repolarization, slow sub-threshold response, fast accommodation, front dissipation, variable peak voltage and other features of cardiac excitability crucial for understanding and controlling arrhythmogenesis [9] where most other ad hoc conceptual equations often fail.

In order to be practically useful beyond its utility as a conceptual tool, the parameter values of the archetypal model [9] must be determined so that it replicates the behaviour of state-of-the-art models of ventricular and atrial excitation and captures experimental measurements quantitatively. This is the goal of the present work. To this end we describe in the following the implementation of a standard parameter estimation procedure and use it to fit the archetypal model to a typical mammalian ventricular model [26], a typical human atrial model [15], as well as to experimental data for rabbit ventricular myocytes available from the literature [27]. In addition, we provide an open-source numerical code permanently available at [4] that can be used by the reader to apply the methodology to other detailed models and data of their own interest. Apart from the computational and conceptual advantages already mentioned, fitting data and detailed models to a common set of equations gives the opportunity to compare and contrast such models directly, which is otherwise impossible due to their different mathematical structure and components. In addition, from a software engineering viewpoint it could be very beneficial when implementing large-scale tissue and whole-heart computational models to be

able to describe different cell types, e.g. ventricular, atrial, sinoatrial, etc., using a single set of equations that only differ by the parameter values employed in various spatial positions.

Model formulation and methods of parameter estimation

The archetypal cardiac cell model

Cardiac cell membranes are composed of a biphospholipid layer, impermeable to charged particles and maintaining a non-zero equilibrium voltage potential across the membrane [44]. The layer is protruded by voltage-gated ion channels – large proteins that open and close depending on the instantaneous value of the voltage and allow in/outflux of ion currents. When a cell is “excited”, these currents cause the formation of a large transmembrane voltage excursion known as an action potential. The action potential propagates within the myocardium and signals cardiac cell contraction thus controlling the heartbeat – the main function of a living heart. To a first approximation the physiology of cell membranes can be modelled as an electrical circuit consisting of a capacitor C_m representing the biphospholipid layer, and an active resistor supporting ionic currents $I_{\text{ion}}(E)$ representing ionic channels, that are connected in parallel, giving rise to the ordinary differential equation $C_m \dot{E} = I_{\text{ion}}(E)$ for the transmembrane voltage potential $E(t)$ [19]. The models of the ionic current $I_{\text{ion}}(E)$ encapsulate the electrophysiological properties of the cardiac membrane mentioned above and over the last 70 years have grown to a staggering complexity as discussed in the Introduction.

Here, we consider the following archetypal model for the action potential of a single cardiac cell

$$\frac{d}{dt}E = \frac{1}{\varepsilon_1 \varepsilon_2} G_{\text{Na}} (E_{\text{Na}} - E) \theta(E - E_*) h + \frac{1}{\varepsilon_2} (g_2(E) n + G(E)), \quad (1a)$$

$$\frac{d}{dt}h = \frac{1}{\varepsilon_1 \varepsilon_2} f_h (\theta(E_{\dagger} - E) - h), \quad (1b)$$

$$\frac{d}{dt}n = F_n(E) (\theta(E - E_{\dagger}) - n). \quad (1c)$$

The model takes the form of a set of piecewise-linear ordinary differential equations for the evolution in time t of three state variables – the voltage E , and the gating variables h and n describing the inactivation of the fast inward and slow outward currents, respectively. Here $\theta(\cdot)$ is the Heaviside step function and

$$g_2(E) = g_{21} \theta(E_{\dagger} - E) + g_{22} \theta(E - E_{\dagger}), \quad F_n(E) = f_n (r \theta(E_{\dagger} - E) + \theta(E - E_{\dagger})), \quad (1d)$$

$$G(E) = \begin{cases} k_1 (E_1 - E), & E \in (-\infty, E_{\dagger}), \\ k_2 (E - E_2), & E \in [E_{\dagger}, E_*], \\ k_3 (E_3 - E), & E \in [E_*, +\infty), \end{cases} \quad (1e)$$

$$E_2 = (k_1/k_2 + 1) E_{\dagger} - E_1 k_1/k_2, \quad E_3 = (k_2/k_3 + 1) E_* - E_2 k_2/k_3. \quad (1f)$$

Equations (1a) to (1c) are integrated in time starting from the initial conditions

$$E(0) = E_{\text{stim}} > E_*, \quad h(0) = 1, \quad n(0) = 0, \quad (1g)$$

and then advancing the solution via a sequence of initial value problems on time intervals $t \in (kB, (k+1)B]$, $k = 1, 2, \dots$ with duration B (basic cycle length), and with initial conditions

$$E(kB) = E_{\text{stim}}, \quad h(kB) = h((k-1)B), \quad n(kB) = n((k-1)B). \quad (1h)$$

The archetypal model (1) was first introduced in [9] as an asymptotic embedding of the original Noble purkinje fiber equations [37] using a set of verifiable transformations with simplification errors that can be measured and controlled accurately. For full details we refer to [9], and here we only note briefly that the asymptotic embedding procedure takes into account the following empirical properties that the original Noble model has in common with the vast majority of other detailed ionic current models: (a) the large differences in the time-scales for evolution of state variables, (b) the large maximal value of the sodium current I_{Na} compared with other currents and (c) the quasi-stationary permeability of the I_{Na} ionic gates in certain potential ranges. Equations (1) differ from the system introduced in [9] only in that n instead of n^4 is used in equation (1a), with the goal to obtain a fully linear system with even simpler closed-form solutions and because parameter values will be adjusted anyway as discussed further below. The archetypal model (1) has already been used to derive asymptotic expressions for the conduction velocity restitution in cardiac tissues [45], to understand the formation of excitation waves [8], and most recently its fast-time subsystem was employed to elucidate the conditions for arrhythmogenesis and refractoriness in atrial tissue with myocyte-fibroblast coupling [32, 33].

Problem (1) has 17 free parameters. Four of them are not intrinsic: $\varepsilon_1, \varepsilon_2, E_{stim}$ and B . The positive constants $\varepsilon_1, \varepsilon_2 \in [0, 1]$ are asymptotic parameters embedded in the model to enable formal asymptotic analysis but both will be kept fixed to unity in the present study. The stimulus voltage E_{stim} and the basic cycle length B are typically specified as a part of an external periodic cell stimulation protocol, also cf. equation (3) below. The remaining 13 parameters are intrinsic to equations (1a) to (1f) and we represent them as the components of a column vector

$$\mathbf{p} = [k_1, k_2, k_3, E_1, E_{Na}, E_{\dagger}, E_*, f_h, f_n, r, G_{Na}, g_{21}, g_{22}]^T. \quad (2)$$

The objective of the study is to find appropriate values for these parameters as discussed next.

Target models and experimental data

We seek to estimate the values of the protocol-independent parameters (2) of the archetypal model (1) so that the model outputs reproduce the behaviour and the biomarkers of target detailed ionic models or experimental measurements. Here, as target models/data we consider the models of Noble [37], Luo-Rudy [26], and Courtemanche [15], as well as the measurements of [27] for rabbit ventricular myocytes.

The Noble model [37] describes the action potential of Purkinje fibre cells. It incorporates a sodium current and two different types of potassium current. The model is based on the Hodgkin-Huxley formulation adjusted to the action potential of Purkinje cells, which is significantly different from that of the squid giant axon in terms of plateau duration. This model is the first ever mathematical model of the action potential of cardiac myocytes and is the ancestor of most current detailed ionic models and the basis of the archetypal model (1).

The Luo-Rudy (LR) model [26] captures the single-cell ventricular action potential of guinea pigs. It includes six ionic currents (sodium, slow inward, time-dependent, time independent and plateau potassium currents and a background current) controlled by seven gate variables and a description of the intracellular calcium concentration.

The Courtemanche et al. (CRN) model [15] describes the action potential of human atrial myocytes. It has 13 ionic currents including formulations of K^+ , Na^+ and Ca^{2+} currents and representations of pump, exchange and background currents. The model is capable of responding to rate changes, calcium channel inhibition and sodium-calcium pump exchanger blockade.

Machine readable implementations of three mathematical models are available from the CellML model repository [30], and are also included with our code [4]. The models are supplemented by stimuli currents $I_{\text{stim}}(t)$ that take the form of periodic trains of rectangular impulses with amplitude I_s , duration t_s , and period (basic cycle length) B ,

$$I_{\text{stim}}(t) = I_s \left[1 + \text{sgn} \left(\sin \frac{\pi t}{B} \right) \text{sgn} \left(\sin \frac{\pi(t - B - 2t_s)}{B} \right) \right]. \quad (3)$$

The inclusion of these currents is known as “stimulation by current”. The currents are used to excite action potentials in the same way as in an experiment and provide an equivalent alternative to the “stimulation by voltage” given by equations (1g) and (1h) for the archetypal model.

The experimental recordings of [27] consist of measurements of action potential and intracellular calcium transient characteristics in isolated myocytes from sub-epicardial, mid-myocardial and sub-endocardial regions of the rabbit left ventricles. These measurements were recorded under both healthy and heart failure conditions. Results showed that in the heart failure group, AP duration and calcium transient duration were prolonged in both sub-epicardial and mid-myocardial cells. These changes were significant at lower stimulus frequencies but the relative effect diminished at higher frequencies. Below we will only consider the measurements of mid-myocardium cells in both healthy and failing myocytes.

Numerical solution and biomarkers

The archetypal model (1) and each of the three target models are integrated in time with a relative tolerance of 10^{-6} employing an adaptive-step, adaptive-order method for systems of stiff ordinary differential equations based on the numerical differentiation formulas of [43] as implemented in Matlab(TM) [49] functions `ode15s` and `ode23`. The resting states of the three target models were used as their respective initial conditions. While a closed-form analytic solution of the archetypal models is available [9], a numerical solution is used here for consistency with the target models.

The following biomarkers are computed for each model.

1. Discretized voltage trace during the k -th basic cycle length period $t \in (kB, (k+1)B]$. More precisely, for the archetypal model this takes the form of a set of ordered pairs $\{(t_{ki}, E_{ki}), i = 0, \dots, M\}$, consisting of discrete values of time $t_{ki} = kB + i \Delta t$ and discrete values of the voltage $E_{ki} = E(t_{ki})$ and $M = B/\Delta t$. A step of $\Delta t = 0.1$ ms is used which is sufficient to resolve the traces.
2. Action potential duration at 90% of the voltage peak amplitude in the k -th basic cycle length period $\mathcal{I} = (kB, (k+1)B]$, defined as the solution A_k of the equation

$$E(A_k + kB) = 0.9 \left(\max_{t \in \mathcal{I}} E(t) - \min_{t \in \mathcal{I}} E(t) \right), \quad (4)$$

that satisfies the condition $\dot{E}(A_k + kB) < 0$. We refer to this biomarker as APD_{90} , an abbreviation often used in the experimental and the physiological literature.

The same type of biomarkers are also available from the experimental measurements of McIntosh et al [27]. Their values were extracted from the published manuscript using the online tool WebPlotDigitizer [41].

Parameter estimation

Having defined appropriate biomarkers, we now compare the archetypal model (1) to each of the target models and the experimental data using a residual (also known in the literature as “error” or “cost” or “objective”) function of the form

$$R(\mathbf{p}) = \frac{1}{2} \left(\left| \frac{A(\mathbf{p}) - \mathcal{A}}{\mathcal{A}} \right| + \frac{1}{M+1} \sum_{i=0}^M \left| \frac{E_i(\mathbf{p}) - \mathcal{E}_i}{\max_{j=0..M} \mathcal{E}_j - \min_{j=0..M} \mathcal{E}_j} \right| \right). \quad (5)$$

Here, E_i are the discrete values of the voltage trace, A is the APD_{90} of the archetypal model while the calligraphic symbols \mathcal{E}_i and \mathcal{A} denote the corresponding values for the target models and data. In particular, the biomarkers in the initial basic cycle period $k = 0$ are used and, for brevity, the subscript k is omitted. This form of the residual measures the discrepancy in the morphologies of the action potentials between the archetypal and the target models/data. The first term of the residual allows the fitting algorithm to assign extra weight to matching the value of APD_{90} when optimising action potential morphology. We remark that, in general, for a complete comparison of the models, the residual needs to include differences between all dynamical variables of the models compared, including all gating variables and ion concentrations. This however, is not possible because of the difference in model formulations, in particular, because different models include different ionic currents and have different dynamical variables. Similarly, model quantities are not easily measured in experiments. The voltage is often the only quantity in common between different models and between models and data.

We now compute parameter values $\tilde{\mathbf{p}}$ of the archetypal model (1) such that the residual (5) is minimised, in symbolic form,

$$\tilde{\mathbf{p}} = \arg \min_{\mathbf{p} \in \Omega} R(\mathbf{p}), \quad (6)$$

where $\Omega \subset \mathbb{R}^{13}$ is the ball $|\mathbf{p} - \mathbf{p}_0| < \tau$ centred at the default values \mathbf{p}_0 of the archetypal model parameters given in the second column of Table 1 and radius $\tau = |\mathbf{p}_0|$. More explicitly, for the parameter estimation function $\arg \min(\cdot)$, we use a MATLAB implementation [17] of the bounded gradient-free Nelder-Mead simplex method [35, 25] for minimisation of real-valued multivariate functions.

We provide an open-source numerical code including the models and methods described in this section. The code is permanently available at [4] and can be used by the readers to reproduce the results described below and/or to apply the methodology to other detailed models and data of their own interest.

Results and discussion

Parameter sensitivity analysis

Prior to estimating the parameter values (2) of the archetypal model (1), we perform a local sensitivity analysis in order to observe how each parameter affects the action potential morphology and to establish whether it is necessary to include all thirteen of them in the optimization search (6). A formal local sensitivity analysis, see e.g. [46], involves computing a sensitivity matrix \mathbf{S} whose entries $S_{ij}(t)$ describe the normalised effect of perturbing the j -th parameter on the i -th state-variable, defined as

$$S_{ij}(t) \equiv \frac{p_{j,0}}{x_i(t; \mathbf{p}_0)} \left[\frac{\partial x_i(t; \mathbf{p})}{\partial p_j} \right]_{\mathbf{p}=\mathbf{p}_0} = \left[\frac{\partial \log x_i(t; \mathbf{p})}{\partial \log p_j} \right]_{\mathbf{p}=\mathbf{p}_0}, \quad \mathbf{x} = [E, h, n]^T. \quad (7)$$

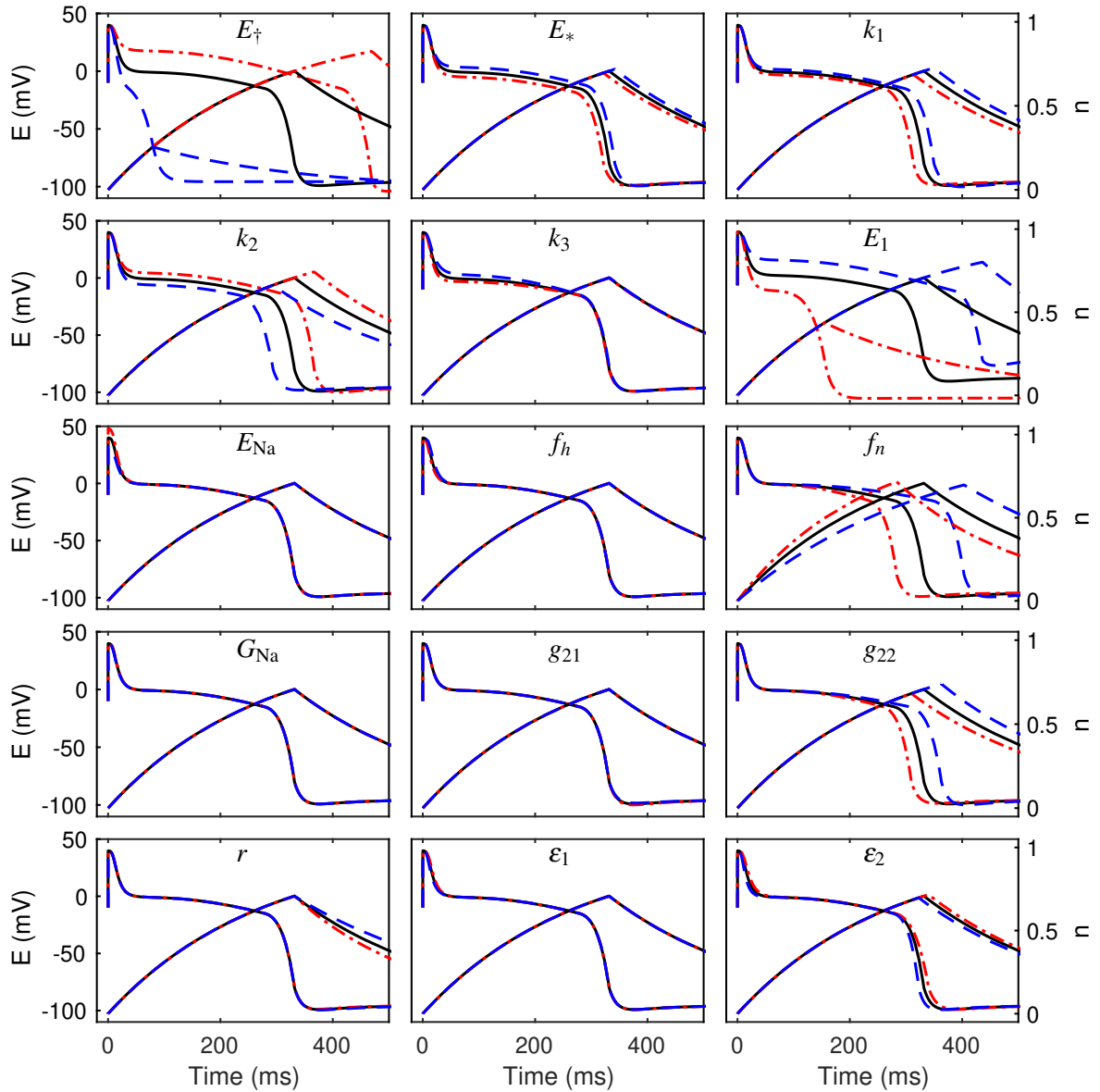


Figure 1: Sensitivity of the profiles of the voltage E and the slow gating variable n of archetypal model (1) to the variation of a single parameter as denoted by the corresponding symbol in each panel. In all panels, the model outputs generated from the default parameter values in Table 1 are shown by solid black line. The dashed blue line and dash-dotted red line are the model outputs obtained with -20% and $+20\%$ perturbation from the default, respectively.

However for clarity, instead of illustrating the elements of the sensitivity matrix, we employ a simpler and more intuitive approach. We vary the value of each of the thirteen model parameters by $\pm 20\%$ from their default values listed in the second column of Table 1 at all other parameter values fixed and observe how this variation affects the traces of the voltage E and the slow gating variable n . Figure 1 illustrates the results from this experiment and also serves to illustrate clearly the effect each of the parameters has on the action potential morphology. For example, the peak membrane potential (PMP) is controlled by the value of E_{Na} while the resting membrane potential (RMP) is influenced by E_1 only. Some of the parameter values affect the

(a) Parameter values						
Params, p_i	Default	Noble [37]	LR [26]	CRN [15]	Healthy [27]	Failing [27]
G_{Na} [ms^{-1}]	100/3	100/3	100/3	100/3	100/3	100/3
E_{Na} [mV]	40.0	40.0	45.0	24.3	41.5	41.5
E_{\dagger} [mV]	-80.0	-80.0	-75.0	-60.0	-80.0	-78.0
E_* [mV]	-15.0	-10.0	11.5	-9.0	20.0	20.0
k_1	0.075	0.04932	0.03602	0.01702	0.0231	0.0173
k_2	0.04	0.03033	0.00443	0.007173	0.0057	0.0068
k_3	0.10	0.08007	0.33946	0.99977	0.0471	0.031
E_1 [mV]	-93.333	-95.667	-84.333	-81.667	-245/3	-245/3
f_n [ms^{-1}]	0.0037	0.004471	0.003781	0.00353	0.0043	0.0040
f_h [ms^{-1}]	0.5	0.5	0.5	0.5	0.5	0.5
g_{21} [$mVms^{-1}$]	-1.0	-0.28325	-0.14359	-0.02303	0.0409	0.0405
g_{22} [$mVms^{-1}$]	-9.0	-2.15744	-0.36512	-0.25370	-1.097	-0.9461
r	1.0	0.7	1.8	2.8	0.4	0.6
(b) Residual error of AP morphology (5)						
$R(\mathbf{p})$	-	0.0067	0.0250	0.0235	0.0155	0.0118

Table 1: Estimates of the parameter values of the archetypal model (1) to selected target models and data as described in text. (a) Parameter values fitted by (6). (b) The residual error in action potential morphology (5) between the archetypal model and targeted models/data. The time is measured in ms, other units are given in the table if dimensional.

action potential morphology in a more complex way. For instance, E_* , E_{\dagger} , g_{22} and f_n control repolarisation, but E_* and E_{\dagger} also contribute to the duration of the plateau. The fast gating variable h exhibits negligible variation from its quasi-stationary value $\bar{h} = 1$ apart from two very short time intervals during the front and the back of the action potential and for this reason is not included in Figure 1.

Parameter estimation

Table 1 lists the results of applying the minimisation procedure (6) to estimate the parameter values (2) of the archetypal model (1) so that it closely reproduces the action potential morphology of the target models [37, 26, 15] and the target data [27]. The agreement obtained in action potential morphology between the archetypal model and the targets is shown in Figure 2. Target models and the archetypal model were stimulated at a basic cycle length $B = 1500$ ms. The archetypal model is able to capture the action potential morphologies of all target models and data used well. The fits of the archetypal model to the CRN [15] and the LR [26] models show the biggest discrepancy as seen in Table 1(b) and Figures 2(b) and (c). The discrepancies are most significant in the neighbourhoods of the post overshoot drop and plateau regions. In particular, the archetypal model is somewhat inaccurate in capturing the deep notch produced by the CRN [15] model. This occurs because the archetypal model lacks transient outward currents K^+ and Na^+/Ca^{2+} exchanger currents [42, 40] that act to form notch phase in the CRN [15] model. The fit of the archetypal model to the Noble model [37] is rather satisfactory. The peak voltage is controlled by the fast sodium current. The peak voltage differs in different regions of the heart due to variation in magnitude of the sodium current. In the archetypal model, the magnitude of the fast inward current is modulated by parameter E_{Na} only. The higher the peak voltage, the higher the value of E_{Na} . This is consistent with our finding (Figure 2 and Table 1), where the LR [26] model has the highest E_{Na} because the model exhibits the largest action

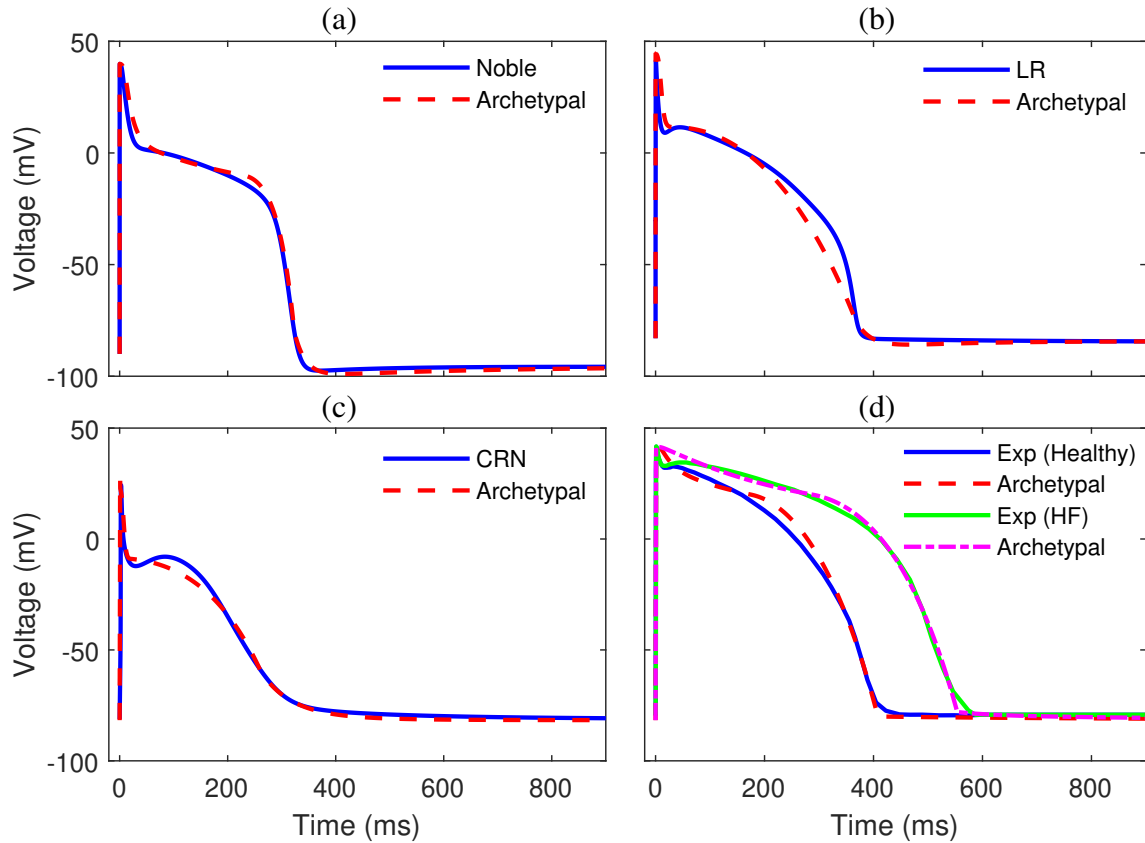


Figure 2: Agreement in action potential morphology between the archetypal model at parameter values listed in Table 1 (broken lines) and corresponding target models (panels (a)-(c), solid lines) and experimental data (panel (d), solid lines). Model names are specified in the panel legends.

potential amplitude. Plateau phase is the long phase of the action potential during which the membrane potential remains depolarised and changes more slowly. This occurs due to balance between some inward and outward currents [42]. In the archetypal model, E_* is one of the parameters that controls the voltage value at the plateau region. The estimated value is consistent for each model, where E_* in the LR [26] model is the biggest since the LR model has the largest value of voltage during this phase, while the smallest is shown by the Noble model.

To fit the archetypal model to isolated cardiac ventricular cell data we use a pacing rate of 0.3Hz ($B = 3333$ ms) at both healthy and heart-failure conditions as this is the basic cycle length employed in [27]. Figure 2(d) shows the action potential morphologies after the fitting process and the new estimated parameter values are shown in last two columns of Table 1. Overall, the archetypal model exhibits good correspondence with the targeted data, with minor discrepancies in the plateau region. The average relative error between the action potentials is relatively small as seen in Table 1(b). Figure 3(c) shows that after fitting the archetypal model to heart-failure data the parameter values most strongly affected are those related to the n gating variable (the slow-gating potassium channels), namely k_1 , k_2 , k_3 , r and g_{22} . These parameters need to be adjusted in order to compensate the large APD₉₀ exhibited in the heart-failure group, which is commonly reported due to down-regulation of potassium current [7, 1]. Other archetypal parameter values like E_{Na} and E_1 are similar in both heart-failure and healthy cells since the

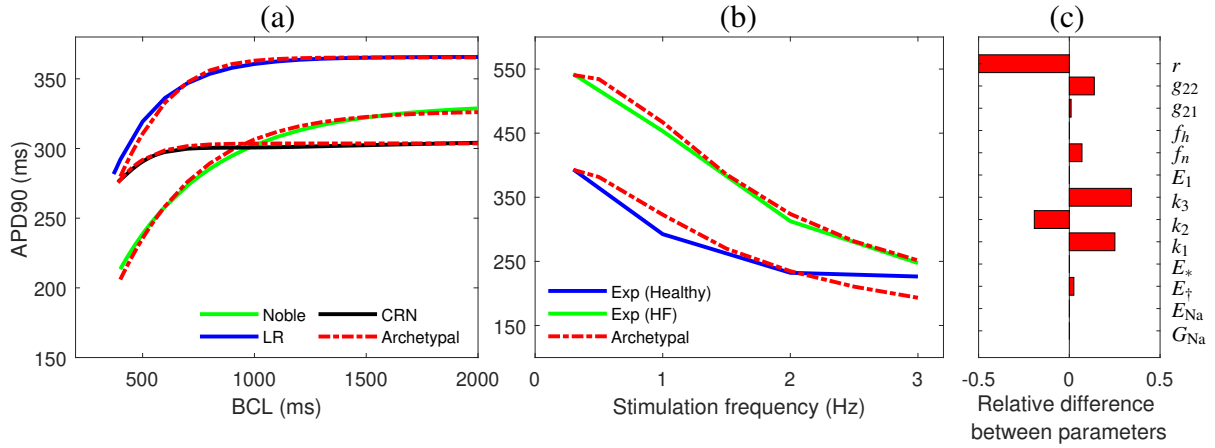


Figure 3: (a,b) APD restitution curves for the archetypal model (dash-dotted line) compared to APD restitution curves of target models/data (solid lines coloured as specified in panel legends). (c) Relative difference between the set of archetypal model parameter values corresponding to experimental measurements in cells from healthy and heart-failure groups.

action potentials have identical amplitude and resting membrane potential.

Tests of APD restitution and computational speedup

In order to test the validity of our parameter estimation results beyond the conditions at which they are obtained, we compare the action potential duration (APD) restitution curves for each of the target models and the experimental data to corresponding curves computed using the parameter estimates reported in Table 1. Figure 3(a) demonstrates excellent agreement between the restitution curves of the authentic target models and the fitted archetypal models, while Figure 3(b) shows similarly good agreement with the restitution curves of the cells from healthy and heart-failure groups. In particular, at a given stimulation frequency failing myocytes exhibit larger APD₉₀ than healthy myocytes. At high stimulation frequency the APD₉₀ values for both groups show a less pronounced difference. The archetypal model is slightly better able to reproduce the accurate APD restitution curve for the HF myocyte, compared to healthy myocyte. For healthy myocyte, the discrepancy occurs at several stimulation frequencies, and it gets pronounced at stimulation frequency larger than 2 Hz, where the archetypal model produces smaller APD₉₀ than the experimental data from healthy myocytes.

Because of the practical value of APD restitution curves, it is important that the fitted archetypal model is able to reproduce the restitution behaviour of the target models and data. These curves describe the dependence of the APD on the duration of the preceding diastolic interval (DI). Nolasco and Dahlen [38] noted that in a single-cell setting and with a fixed period of excitation, a slope of the APD(DI) curve greater than one indicates instability of the train of action potentials. For this reason, the restitution curves are considered an important tool in understanding instabilities of excitation waves leading to onset of cardiac arrhythmias [52] and is routinely measured experimentally, e.g. in the experimental work [27] that we compare with.

In order to quantify the computational speedup gained by using the archetypal model with fitted parameter values in comparison with authentic target models we measured the time taken using each model to compute numerically a train of 1000 action potentials at a fixed value of the basic cycle length $B = 1000$ ms. With the numerical methods described above in the paper, the archetypal model takes approximately about 180 sec to complete the numerical simulation with any set of parameter values. The LR [26] and CRN [15] model require 1246 sec and 1634

sec, respectively for the same simulation. Thus we conclude that using the archetypal model is 6 times faster than using the Luo-Rudy model [26] and 9 times faster than the using Courtemanche et al. model [15]. In simulations of whole-heart or 3D tissue with realistic geometries, this will reduce the computational workload and runtime significantly. The numerical speedup advantage of using the archetypal model is likely even more pronounced in case of comparison with contemporary models more detailed than the LR [26] and the CRN [15] models. We also recall that the archetypal has closed form solutions that can be evaluated directly irrespective of parameter values used and this can be exploited to further reduce computational expenses or even eliminate the need of computation entirely.

Summary and conclusion

Contemporary mathematical models of single-cell cardiac electrical excitation have become immensely detailed. Along with increasing physiological realism such model complexity leads to parameter uncertainty, high computational cost and barriers to mechanistic understanding. There is thus a need for conceptually and mathematically simple but physiologically accurate reduced models of the cardiac action potential. A single-cell cardiac excitation model that replicates the phase-space geometry of detailed cardiac models but is much simpler in both functional form and number of free parameters was derived in [9] and applied to a number of idealised problems [45, 8, 32, 33]. In order to render the archetypal model of [9] also practically applicable to the description of physiological measurements and to whole-heart and tissue numerical simulations, in this study we report a robust method for estimation of the parameter values of the model so as to approximate the action potential biomarkers of contemporary detailed ionic models as well as experimental data from direct wet-lab cell measurements. The parameter estimation procedure relies on the well-known and popular Nelder-Mead method [35] for minimisation of multi-variable functions by direct simplex search. Here, the optimal parameter values of the archetype are determined by minimising the residual difference between the morphologies of single-stimulus action potentials of the archetypal model and the target model/data. The procedure is then applied to 5 test cases, namely (a) to the authentic Noble model [37], the precursor to all detailed cardiac ionic current models; (b) to the Luo-Rudy ventricular cell model [26], the original second generation model; (c) to the Courtemanche, Ramirez and Natel atrial cell model [15], a popular modern cardiac system, as well as (d,e) to wet lab experimental measurements of rabbit ventricular cells from both healthy and heart-failure samples [27]. In all cases, sets of values of the archetypal model parameters have been found so that the morphologies of stable single-stimulus action potential target transients are well reproduced. As this is an optimisation problem in high-dimensional parameter space that may have several local minima, it is difficult to ascertain if a given solution of the minimisation procedure using Nelder-Mead method is the best possible one. To further test and validate the method, action potential duration restitution curves are also computed and compared to those of the target models and data, again with excellent agreement. We conclude that compared to more sophisticated parameter estimation methods for cardiac models such as maximum-likelihood estimation [29], principal-axis fitting [54], genetic algorithms [47, 24], as well as the widely practised empirical “hand-tuning” of free parameters [5, 28], our rather straightforward approach provides comparable quality of approximation and performs remarkably well. This is likely due to the generic structure and the small number of parameters of the archetypal model we consider. An open-source Matlab(TM) implementation of the models and methods is made permanently available at [4] and can be used by the readers to fit the archetypal model to models and data of their own choice.

Acknowledgements

This work was supported by the UK Engineering and Physical Sciences Research Council [EP-SRC grant numbers EP/N014642/1, EP/S030875/1, EP/T017899/1]. M.H.N. Aziz was funded by the Ministry of Higher Education Malaysia and University of Malaya under a SLAB scholarship.

References

1. Akar, F. G. & Rosenbaum, D. S. (2003). Transmural Electrophysiological Heterogeneities Underlying Arrhythmogenesis in Heart Failure. *Circulation Research*, 93(7), 638–645, doi:[10.1161/01.res.0000092248.59479.ae](https://doi.org/10.1161/01.res.0000092248.59479.ae).
2. Aliev, R. R. & Panfilov, A. V. (1996). A simple two-variable model of cardiac excitation. *Chaos, Solitons & Fractals*, 7(3), 293–301, doi:[10.1016/0960-0779\(95\)00089-5](https://doi.org/10.1016/0960-0779(95)00089-5).
3. Amanfu, R. K. & Saucerman, J. J. (2011). Cardiac Models in Drug Discovery and Development: A Review. *Critical Reviews in Biomedical Engineering*, 39(5), 379–395, doi:[10.1615/critrevbiomedeng.v39.i5.30](https://doi.org/10.1615/critrevbiomedeng.v39.i5.30).
4. Aziz, M. H. N. & Simitiev, R. D. (2021). Code for Estimation of Parameters for an Archetypal Model of Cardiomyocyte Membrane Potentials. *Zenodo*, doi:[10.5281/zenodo.4568662](https://doi.org/10.5281/zenodo.4568662).
5. Baranauskas, G. (2006). Sodium Currents Activate without a Hodgkin and Huxley-Type Delay in Central Mammalian Neurons. *Journal of Neuroscience*, 26(2), 671–684, doi:[10.1523/jneurosci.2283-05.2006](https://doi.org/10.1523/jneurosci.2283-05.2006).
6. Bassingthwaite, J. B. (2000). Strategies for the Physiome Project. *Annals of Biomedical Engineering*, 28(8), 1043–1058, doi:[10.1114/1.1313771](https://doi.org/10.1114/1.1313771).
7. Beuckelmann, D. J., Näbauer, M., & Erdmann, E. (1993). Alterations of K⁺ currents in isolated human ventricular myocytes from patients with terminal heart failure. *Circulation Research*, 73(2), 379–385, doi:[10.1161/01.res.73.2.379](https://doi.org/10.1161/01.res.73.2.379).
8. Bezekci, B., Idris, I., Simitiev, R. D., & Biktashev, V. N. (2015). Semianalytical approach to criteria for ignition of excitation waves. *Physical Review E*, 92(4), doi:[10.1103/physreve.92.042917](https://doi.org/10.1103/physreve.92.042917).
9. Biktashev, V. N., Suckley, R., Elkin, Y. E., & Simitiev, R. D. (2008). Asymptotic Analysis and Analytical Solutions of a Model of Cardiac Excitation. *Bulletin of Mathematical Biology*, 70(2), 517–554, doi:[10.1007/s11538-007-9267-0](https://doi.org/10.1007/s11538-007-9267-0).
10. Biktasheva, I., Simitiev, R., Suckley, R., & Biktashev, V. (2006). Asymptotic properties of mathematical models of excitability. *Philosophical Transactions of the Royal Society A: Mathematical, Physical and Engineering Sciences*, 364(1842), 1283–1298, doi:[10.1098/rsta.2006.1770](https://doi.org/10.1098/rsta.2006.1770).
11. Clayton, R., et al. (2011). Models of cardiac tissue electrophysiology: Progress, challenges and open questions. *Progress in Biophysics and Molecular Biology*, 104(1-3), 22–48, doi:[10.1016/j.pbiomolbio.2010.05.008](https://doi.org/10.1016/j.pbiomolbio.2010.05.008).
12. Clayton, R. H., et al. (2020). An audit of uncertainty in multi-scale cardiac electrophysiology models. *Philosophical Transactions of the Royal Society A: Mathematical, Physical and Engineering Sciences*, 378(2173), 20190335, doi:[10.1098/rsta.2019.0335](https://doi.org/10.1098/rsta.2019.0335).
13. Clerx, M., Beattie, K. A., Gavaghan, D. J., & Mirams, G. R. (2019). Four Ways to Fit an Ion Channel Model. *Biophysical Journal*, 117(12), 2420–2437, doi:[10.1016/j.bpj.2019.08.001](https://doi.org/10.1016/j.bpj.2019.08.001).
14. Cooper, J., Scharm, M., & Mirams, G. R. (2016). The Cardiac Electrophysiology Web Lab. *Biophysical Journal*, 110(2), 292–300, doi:[10.1016/j.bpj.2015.12.012](https://doi.org/10.1016/j.bpj.2015.12.012).
15. Courtemanche, M., Ramirez, R. J., & Nattel, S. (1998). Ionic mechanisms un-

- derlying human atrial action potential properties: insights from a mathematical model. *American Journal of Physiology-Heart and Circulatory Physiology*, 275(1), H301–H321, doi:[10.1152/ajpheart.1998.275.1.h301](https://doi.org/10.1152/ajpheart.1998.275.1.h301).
16. Davies, M. R., et al. (2016). Recent developments in using mechanistic cardiac modelling for drug safety evaluation. *Drug Discovery Today*, 21(6), 924–938, doi:[10.1016/j.drudis.2016.02.003](https://doi.org/10.1016/j.drudis.2016.02.003).
 17. D’Errico, J. (2021). `fminsearchbnd`, `fminsearchcon`, MATLAB Central File Exchange, www.mathworks.com/matlabcentral/fileexchange/8277-fminsearchbnd-fminsearchcon.
 18. Fenton, F. & Karma, A. (1998). Vortex dynamics in three-dimensional continuous myocardium with fiber rotation: Filament instability and fibrillation. *Chaos: An Interdisciplinary Journal of Nonlinear Science*, 8(1), 20–47, doi:[10.1063/1.166311](https://doi.org/10.1063/1.166311).
 19. Fenton, F. H. & Cherry, E. M. (2008). Models of cardiac cell. *Scholarpedia*, 3(8), 1868, doi:[10.4249/scholarpedia.1868](https://doi.org/10.4249/scholarpedia.1868).
 20. FitzHugh, R. (1961). Impulses and Physiological States in Theoretical Models of Nerve Membrane. *Biophysical Journal*, 1(6), 445–466, doi:[10.1016/s0006-3495\(61\)86902-6](https://doi.org/10.1016/s0006-3495(61)86902-6).
 21. Heijman, J., Abdoust, P. E., Voigt, N., Nattel, S., & Dobrev, D. (2015). Computational models of atrial cellular electrophysiology and calcium handling, and their role in atrial fibrillation. *The Journal of Physiology*, 594(3), 537–553, doi:[10.1113/jp271404](https://doi.org/10.1113/jp271404).
 22. Iyer, V., Mazhari, R., & Winslow, R. L. (2004). A Computational Model of the Human Left-Ventricular Epicardial Myocyte. *Biophysical Journal*, 87(3), 1507–1525, doi:[10.1529/biophysj.104.043299](https://doi.org/10.1529/biophysj.104.043299).
 23. Johnstone, R. H., et al. (2016). Uncertainty and variability in models of the cardiac action potential: Can we build trustworthy models? *Journal of Molecular and Cellular Cardiology*, 96, 49–62, doi:[10.1016/j.yjmcc.2015.11.018](https://doi.org/10.1016/j.yjmcc.2015.11.018).
 24. Kaur, J., Nygren, A., & Vigmond, E. J. (2014). Fitting Membrane Resistance along with Action Potential Shape in Cardiac Myocytes Improves Convergence: Application of a Multi-Objective Parallel Genetic Algorithm. *PLoS ONE*, 9(9), e107984, doi:[10.1371/journal.pone.0107984](https://doi.org/10.1371/journal.pone.0107984).
 25. Lagarias, J. C., Reeds, J. A., Wright, M. H., & Wright, P. E. (1998). Convergence Properties of the Nelder–Mead Simplex Method in Low Dimensions. *SIAM Journal on Optimization*, 9(1), 112–147, doi:[10.1137/s1052623496303470](https://doi.org/10.1137/s1052623496303470).
 26. Luo, C. H. & Rudy, Y. (1991). A model of the ventricular cardiac action potential. Depolarization, repolarization, and their interaction. *Circulation Research*, 68(6), 1501–1526, doi:[10.1161/01.res.68.6.1501](https://doi.org/10.1161/01.res.68.6.1501).
 27. McIntosh, M. (2000). Heterogeneous changes in action potential and intracellular Ca²⁺ in left ventricular myocyte sub-types from rabbits with heart failure. *Cardiovascular Research*, 45(2), 397–409, doi:[10.1016/s0008-6363\(99\)00360-0](https://doi.org/10.1016/s0008-6363(99)00360-0).
 28. Mickus, T., Yoon Jung, H., & Spruston, N. (1999). Properties of Slow, Cumulative Sodium Channel Inactivation in Rat Hippocampal CA1 Pyramidal Neurons. *Biophysical Journal*, 76(2), 846–860, doi:[10.1016/s0006-3495\(99\)77248-6](https://doi.org/10.1016/s0006-3495(99)77248-6).
 29. Milescu, L. S., Akk, G., & Sachs, F. (2005). Maximum Likelihood Estimation of Ion Channel Kinetics from Macroscopic Currents. *Biophysical Journal*, 88(4), 2494–2515, doi:[10.1529/biophysj.104.053256](https://doi.org/10.1529/biophysj.104.053256).
 30. Miller, A. K., et al. (2010). An overview of the CellML API and its implementation. *BMC Bioinformatics*, 11(1), doi:[10.1186/1471-2105-11-178](https://doi.org/10.1186/1471-2105-11-178).
 31. Mitchell, C. (2003). A two-current model for the dynamics of cardiac membrane. *Bulletin*

- of *Mathematical Biology*, 65(5), 767–793, doi:[10.1016/s0092-8240\(03\)00041-7](https://doi.org/10.1016/s0092-8240(03)00041-7).
32. Mortensen, P., Gao, H., Smith, G., & Simitev, R. D. (2021a). Action potential propagation and block in a model of atrial tissue with myocyte–fibroblast coupling. *Mathematical Medicine and Biology: A Journal of the IMA*, 38(1), 106–131, doi:[10.1093/imammb/dqaa014](https://doi.org/10.1093/imammb/dqaa014).
 33. Mortensen, P., Gao, H., Smith, G., & Simitev, R. D. (2021b). Addendum: Action potential propagation and block in a model of atrial tissue with myocyte–fibroblast coupling. *Mathematical Medicine and Biology*, doi:[10.1093/imammb/dqab005](https://doi.org/10.1093/imammb/dqab005).
 34. Nagumo, J., Arimoto, S., & Yoshizawa, S. (1962). An Active Pulse Transmission Line Simulating Nerve Axon. *Proceedings of the IRE*, 50(10), 2061–2070, doi:[10.1109/jrproc.1962.288235](https://doi.org/10.1109/jrproc.1962.288235).
 35. Nelder, J. A. & Mead, R. (1965). A Simplex Method for Function Minimization. *The Computer Journal*, 7(4), 308–313, doi:[10.1093/comjnl/7.4.308](https://doi.org/10.1093/comjnl/7.4.308).
 36. Niederer, S. A., Fink, M., Noble, D., & Smith, N. P. (2009). A meta-analysis of cardiac electrophysiology computational models. *Experimental Physiology*, 94(5), 486–495, doi:[10.1113/expphysiol.2008.044610](https://doi.org/10.1113/expphysiol.2008.044610).
 37. Noble, D. (1962). A modification of the Hodgkin-Huxley equations applicable to Purkinje fibre action and pacemaker potentials. *The Journal of Physiology*, 160(2), 317–352, doi:[10.1113/jphysiol.1962.sp006849](https://doi.org/10.1113/jphysiol.1962.sp006849).
 38. Nolasco, J. B. & Dahlen, R. W. (1968). A graphic method for the study of alternation in cardiac action potentials. *Journal of Applied Physiology*, 25(2), 191–196, doi:[10.1152/jappl.1968.25.2.191](https://doi.org/10.1152/jappl.1968.25.2.191).
 39. O'Hara, T., Virág, L., Varró, A., & Rudy, Y. (2011). Simulation of the Undiseased Human Cardiac Ventricular Action Potential: Model Formulation and Experimental Validation. *PLoS Computational Biology*, 7(5), e1002061, doi:[10.1371/journal.pcbi.1002061](https://doi.org/10.1371/journal.pcbi.1002061).
 40. Peñaranda, A., Cantalapiedra, I. R., Bragard, J., & Echebarria, B. (2012). Cardiac dynamics: a simplified model for action potential propagation. *Theoretical Biology and Medical Modelling*, 9(1), doi:[10.1186/1742-4682-9-50](https://doi.org/10.1186/1742-4682-9-50).
 41. Rohatgi, A. (2020). Webplotdigitizer: Version 4.4, <https://automeris.io/WebPlotDigitizer>.
 42. Santana, L. F., Cheng, E. P., & Lederer, W. J. (2010). How does the shape of the cardiac action potential control calcium signaling and contraction in the heart? *Journal of Molecular and Cellular Cardiology*, 49(6), 901–903, doi:[10.1016/j.yjmcc.2010.09.005](https://doi.org/10.1016/j.yjmcc.2010.09.005).
 43. Shampine, L. F. & Reichelt, M. W. (1997). The MATLAB ODE Suite. *SIAM Journal on Scientific Computing*, 18(1), 1–22, doi:[10.1137/s1064827594276424](https://doi.org/10.1137/s1064827594276424).
 44. Sigg, D. C., Iaizzo, P. A., Xiao, Y.-F., & He, B., Eds. (2010). *Cardiac Electrophysiology Methods and Models*. Springer US.
 45. Simitev, R. D. & Biktashev, V. N. (2011). Asymptotics of Conduction Velocity Restitution in Models of Electrical Excitation in the Heart. *Bulletin of Mathematical Biology*, 73(1), 72–115, doi:[10.1007/s11538-010-9523-6](https://doi.org/10.1007/s11538-010-9523-6).
 46. Snowden, T. J., van der Graaf, P. H., & Tindall, M. J. (2017). Methods of Model Reduction for Large-Scale Biological Systems: A Survey of Current Methods and Trends. *Bulletin of Mathematical Biology*, 79(7), 1449–1486, doi:[10.1007/s11538-017-0277-2](https://doi.org/10.1007/s11538-017-0277-2).
 47. Syed, Z., Vigmond, E., Nattel, S., & Leon, L. J. (2005). Atrial cell action potential parameter fitting using genetic algorithms. *Medical & Biological Engineering & Computing*, 43(5), 561–571, doi:[10.1007/bf02351029](https://doi.org/10.1007/bf02351029).

48. ten Tusscher, K. H. W. J., Noble, D., Noble, P. J., & Panfilov, A. V. (2004). A model for human ventricular tissue. *American Journal of Physiology-Heart and Circulatory Physiology*, 286(4), H1573–H1589, doi:[10.1152/ajpheart.00794.2003](https://doi.org/10.1152/ajpheart.00794.2003).
49. The Mathworks, Inc. (2017). *MATLAB version 9.3.0.713579 (R2017b)*. Natick, Massachusetts.
50. Trayanova, N. A., Doshi, A. N., & Prakosa, A. (2020). How personalized heart modeling can help treatment of lethal arrhythmias: A focus on ventricular tachycardia ablation strategies in post-infarction patients. *Wiley Interdisciplinary Reviews: Systems Biology and Medicine*, 12(3), e1477, doi:[10.1002/wsbm.1477](https://doi.org/10.1002/wsbm.1477).
51. Trayanova, N. A., Popescu, D. M., & Shade, J. K. (2021). Machine Learning in Arrhythmia and Electrophysiology. *Circulation Research*, 128(4), 544–566, doi:[10.1161/circresaha.120.317872](https://doi.org/10.1161/circresaha.120.317872).
52. Tse, G., Wong, S. T., Tse, V., Lee, Y. T., Lin, H. Y., & Yeo, J. M. (2016). Cardiac dynamics: Alternans and arrhythmogenesis. *Journal of Arrhythmia*, 32(5), 411–417, doi:[10.1016/j.joa.2016.02.009](https://doi.org/10.1016/j.joa.2016.02.009).
53. van der Pol, B. & van der Mark, J. (1928). LXXII. The heartbeat considered as a relaxation oscillation, and an electrical model of the heart. *The London, Edinburgh, and Dublin Philosophical Magazine and Journal of Science*, 6(38), 763–775, doi:[10.1080/14786441108564652](https://doi.org/10.1080/14786441108564652).
54. Vandenberg, C. & Bezanilla, F. (1991). A sodium channel gating model based on single channel, macroscopic ionic, and gating currents in the squid giant axon. *Biophysical Journal*, 60(6), 1511–1533, doi:[10.1016/s0006-3495\(91\)82186-5](https://doi.org/10.1016/s0006-3495(91)82186-5).
55. Whittaker, D. G., Clerx, M., Lei, C. L., Christini, D. J., & Mirams, G. R. (2020). Calibration of ionic and cellular cardiac electrophysiology models. *Wiley Interdisciplinary Reviews: Systems Biology and Medicine*, 12(4), e1482, doi:[10.1002/wsbm.1482](https://doi.org/10.1002/wsbm.1482).
56. Wilhelms, M., Hettmann, H., Maleckar, M. M., Koivumäki, J. T., Dössel, O., & Seemann, G. (2013). Benchmarking electrophysiological models of human atrial myocytes. *Frontiers in Physiology*, 3, doi:[10.3389/fphys.2012.00487](https://doi.org/10.3389/fphys.2012.00487).

Muhamad H.N. Aziz

E-mail: hifz_din@um.edu.my



Aziz graduated from the University of Malaya, Malaysia with a Bachelor in Mathematics in 2014, followed by a Master in Applied Mathematics in 2015 from the University of Glasgow, United Kingdom. He recently received his Ph.D in 2021 from the same university in the area of mathematical biology. He currently holds a lecturer position at University of Malaya. His research interest is in the modelling of cardiac electrophysiology, particularly in investigating the cellular heterogeneity and their responses to cardiac antiarrhythmic drugs.

Place here
a photograph
of the author
(no larger than
3 × 4 cm)

Radostin D. SimatevE-mail: Radostin.Simatev@glasgow.ac.uk

Simatev holds a MSc degree in Particle and Nuclear Physics from the University of Sofia, Bulgaria and a Dr Rer Nat degree from the University of Bayreuth, Germany. After a period of post-doctoral research at the University of Liverpool, Simatev joined the School of Mathematics and Statistics at the University of Glasgow, UK where he currently remains. Simatev has held visiting positions at Stanford University, University of California, Los Angeles and the Nordic Institute of Theoretical Physics, Sweden. Simatev works in the area of magnetohydrodynamics and convective dynamo theory, where he has made contributions to modelling of geomagnetic polarity reversals, solar cycles and bistability of turbulent dynamos. Simatev also works in cardiac excitability and arrhythmogenesis where we has used asymptotic methods to investigate absolute refractoriness in atrial tissues, conduction velocity restitution and initiation of excitable waves. Simatev has orcid.org/0000-0002-2207-5789.



© 2018 by the authors. Licensee Institute of Biophysics and Biomedical Engineering, Bulgarian Academy of Sciences. This article is an open access article distributed under the terms and conditions of the Creative Commons Attribution (CC BY) license (<http://creativecommons.org/licenses/by/4.0/>).